



Motility-induced phase separation is reentrant

Jie Su^{1,2}, Mengkai Feng^{1,2}, Yunfei Du¹, Huijun Jiang¹  [✉] & Zhonghuai Hou¹  [✉]

Active Brownian particles (ABPs) with pure repulsion is an ideal model to understand the effect of nonequilibrium on collective behaviors. It has long been established that activity can create effective attractions leading to motility-induced phase separation (MIPS), whose role is similar to that of (inverse) temperature in the simplest equilibrium system with attractive inter-particle interactions. Here, we report that activity can lead to a counterintuitive reentrant MIPS, which is completely different from the phase behavior of equilibrium systems, shown by both simulations and theory. Our theoretical analysis based on a kinetic theory of MIPS shows that an additional term of activity-induced nonequilibrium vaporization is able to hinder the formation of dense phase when activity is large enough. Such effect along with the activity-induced effective attraction thus lead to the MIPS reentrance. Numerical simulations verify this nonequilibrium effect induced solely by activity on phase behaviors of ABPs, and further demonstrate the dependence of MIPS on activity and the strength of inter-particle interaction predicted by our theoretical analysis. Our findings highlight the particular role played by the nonequilibrium nature of activity on phase behaviors of active systems, which may inspire deep insights into the essential difference between equilibrium and nonequilibrium systems.

¹Department of Chemical Physics & Hefei National Research Center for Physical Sciences at the Microscale, University of Science and Technology of China, Hefei 230026 Anhui, China. ²These authors contributed equally: Jie Su, Mengkai Feng. ✉email: hjjiang3@ustc.edu.cn; hzhlj@ustc.edu.cn

Active systems consisting of self-propelled units have been widely discovered in nature on many scales, ranging from mesoscopic biological or manmade swimmers such as *E. coli* and Janus spheres to macroscopic objects like fish, birds and horses^{1,2}. Due to the ability to take in and dissipate energy to drive themselves far from equilibrium³, active systems provide ideal model systems to investigate the effect of nonequilibrium on collective behaviors beyond their equilibrium counterparts^{4–18}. As one of the simplest active systems, active Brownian particles (ABPs) with pure repulsion without any attraction can spontaneously undergo phase separation between dense and dilute fluid phases^{19,20}. Such phase separation resulting solely from the intrinsically nonequilibrium property, i.e., activity, is so-called motility-induced phase separation (MIPS)^{16,19–34}.

Generally, for ABPs with pure repulsion, they tend to accumulate where they move more slowly and will slow down at high density for steric reasons, which then creates effective attractions leading to MIPS²⁰. Quite interestingly, it has been found that the phase diagram of ABPs^{20–23} is nearly the same as that of the simplest equilibrium system with attractive inter-particle interactions^{35–37}, except that the role of (inverse) temperature is replaced by activity. Is that all about the effect of activity on the phase separation of ABPs? Will the nonequilibrium nature of activity bring unique phase behaviors to the simplest ABPs beyond providing an alternative origin for phase separation?

In this work, we report that activity can lead to a unique phase behavior of a counterintuitive MIPS reentrance, which lacks an analog in equilibrium systems. Our theoretical analysis based on a kinetic theory of MIPS in the simplest ABP system with purely repulsive interactions shows that, this phase behavior stems from a new type of nonequilibrium vaporization induced by activity. While activity-induced effective attraction leads to MIPS, activity-induced nonequilibrium vaporization hinders the formation of dense phase and thus results in the MIPS reentrance. Besides, we find that the “softer” the repulsive interaction potential is, the “stronger” the reentrance becomes. In simulations, the reentrant MIPS is confirmed and fits very well with our theory. Specifically, the simulated binodal agrees well with the phase boundary derived by our theoretical analysis, and both simulations and theory give the same relationship between reentrant MIPS and the strength of interactions.

Results and discussion

Theoretical analysis. We start from a minimal active fluid theory characterizing MIPS from a kinetics approach^{21,22,38}. The theory describes the steady state of phase separation with a dense clustering phase which is set as close packed and a dilute phase as homogeneous and isotropic. Particles transport between two phases through condensation and evaporation events with rates k_{in} and k_{out} , respectively. Absorption rate k_{in} is assumed to be proportion to the dilute phase number density ρ_g and the characteristic self-propulsion velocity v_0 . For the vaporization, the theory sets that active particles immediately escape from the dense phase when the direction of the particle on the interface moves towards to dilute phase. Therefore the escape rate k_{out} is proportion to the rotational diffusion constants D_r . Then the steady state condition is achieved through equating k_{in} and k_{out} , leading to the dilute phase density $\rho_g = \frac{\pi \kappa' D_t}{\sigma v_0}$ where κ' is a fitting parameter and σ is the particle diameter. For two dimensional ABP system with purely repulsive inter-particle potential^{21,22} and Lennard–Jones potential³⁸, solutions of ρ_g show very good agreement with simulated MIPS. However, it should be noted that the particle current from cluster to dilute phase comprises

not only vaporization events due to rotational-diffusion-dependent active motion, but also diffusion process along the particle density gradient. Good agreement between solutions of ρ_g and simulated MIPS indicates the former one makes a major contribution to k_{out} for activity ranging around the transition point of MIPS (i.e., small and moderate activity). Yet for large activity, the contribution of diffusion process becomes progressively more important as will be shown by the following analysis.

In general, the diffusion current is proportional to the density gradient $\nabla \rho$ with coefficient D . In the gas phase, the translational diffusion coefficient is close to the effective one for a free active particle $D_0 = D_t + \frac{v_0^2}{2D_r}$, where D_t is purely thermal diffusion constant²⁰ and the second term of rhs is so called “swim diffusivity”³⁹. However, in the dense phase, this diffusion coefficient D is not simply D_t nor D_0 . Inspired by refs. 40,41, wherein an “instantaneous diffusion coefficient” for selected particle- i was introduced to investigate the time evolution of dense ABP system, defined as $D_i = D_t + \frac{v_0^2/(2D_r)}{1 + \frac{v_0^2}{2D_r} \sum_{j \neq i} \nabla_i^2 U(r_{ij})}$, where $U(r_{ij})$ is the inter-particle potential and γ is the friction coefficient. Although this D_i is not a long-time diffusivity that one we desired, it brings a good phenomenological method to estimate D . Based on the formula of D_i , we write the effective diffusion in dense phase as $D = D_t + \frac{\lambda v_0^2}{D_r}$ in the sense of average, with a dimensionless parameter $\lambda \in (0, \frac{1}{2})$ representing the complex interaction. We do notice that the divide of evaporation event and diffusional process, is a little ambiguous and there might be double counting in this context. At least for a single event that a particle leaves the dense phase, it is difficult to determine which type of diffusion plays a major role. Nevertheless, we use a fitting parameter κ to compromise this defect, then the total current leaving dense phase can be written as

$$j_{\text{out}} = D \nabla \rho + \kappa \frac{D_r}{\sigma} \rho_d - \rho_g + \kappa \frac{D_r}{\sigma} \rho_d \quad (1)$$

where ρ_d is the number density of the dense phase. Analogous to the procedure in ref. 21, by integrating the angles of ABPs over the direction of self-propulsion toward the interface, the condensation current is written as $j_{\text{in}} = \rho_g v_0 / \pi$.

Based on the steady-state assumption, i.e., $j_{\text{in}} = j_{\text{out}}$, two transition points can be immediately derived as

$$v_c^\pm = \frac{D_r \sigma}{2\lambda(\rho_d - \rho_g)} \left[\frac{\rho_g}{\pi} \pm \sqrt{\frac{\rho_g^2}{\pi^2} - 4 \frac{\lambda(\rho_d - \rho_g)}{D_r \sigma^2} [D_t(\rho_d - \rho_g) + \kappa D_r]} \right] \quad (2)$$

We recall that, in the previous understanding of MIPS taking only rotational-diffusion-dependent vaporization into account, there is only one transition point v_c , since j_{out} is independent on v_0 and j_{in} increases linearly with v_0 ²¹. Consequently, MIPS will be observed as $v_0 > v_c$, and activity is considered to mainly provide a nonequilibrium origin for phase separation. Quite interestingly, Eq. (2) points out that, increasing activity not only leads to MIPS when v_0 passes v_c^- but also destroys it when $v_0 > v_c^+$. Such reentrant MIPS of the simplest ABPs with purely repulsive inter-particle interactions indicates that, beyond the activity-induced effective attraction when only rotational-diffusion-dependent vaporization is considered, an extra effective diffusivity due to active motion further contributes a contrary effect on phase separation by accelerating melting. Such unique phase behavior induced by the nonequilibrium nature of activity has never been

observed in the equilibrium analogs with attractive inter-particle interactions.

There are several further predictions can be made about the interesting phase behavior. Firstly, the steady state assumption $j_{\text{in}} = j_{\text{out}}$ gives a quantitative measurement of the dilute phase density, $\rho_g = (\rho_d D + \kappa D_r) / (D + \nu_0 \sigma / \pi)$. Unlike the previous theory where dilute phase density decreases with ν_0 non-monotonically, ρ_g eventually increases to ρ_d for very large activity. This result strongly implies a homogeneous state when activity is sufficiently large, which confirms the reentrance of MIPS from another point of view.

Secondly, the parameter λ should be dependent on the repulsive inter-particle potential $U(r) = \epsilon \hat{U}(r)$, where ϵ is the strength of the potential and $\hat{U}(r)$ is a dimensionless inter-particle potentials. Qualitatively, larger ϵ brings stronger repulsive force which hinders particle motion in the dense phase, and consequently leads to smaller λ and smaller diffusivity D . According to Eq. (2), ν_c^+ prominently increases with interacting strength ϵ , while on the contrary ν_c^- slowly decreases. As a result, MIPS would also be reentrant for finite interacting strength ϵ , while increasing ϵ would greatly broaden the parameter region for emergence of MIPS. It is thus another testable prediction of our theory to investigate the dependence of MIPS behavior on the interacting strength.

Numerical simulation. In order to verify the unique phase behavior predicted by the aforementioned theoretical analysis, we perform simulations of a two-dimensional system with size $L_x \times L_y$ and periodic boundary conditions consisting of N spherical ABPs with diameter σ and friction coefficient γ . The pairwise inter-particle potential is set as Weeks–Chandler–Andersen (WCA) potential $U(r_{ij}) = 4\epsilon[(\sigma/r_{ij})^{12} - (\sigma/r_{ij})^6 + 1/4]$ for $r_{ij} < 2^{1/6}\sigma$ and $U(r_{ij}) = 0$ otherwise. We set the translational diffusion coefficient $D_t = k_B T / \gamma$ so that the system satisfies the fluctuation-dissipation relation with k_B the Boltzmann constant and T the temperature. We presume that the rotational diffusion coefficient D_r is coupled with the translational diffusivity as $D_r = 3D_t/\sigma^2$. In this work, we use two dimensionless variables as control parameters, i.e. the Péclet number $\text{Pe} = \nu_0 \sigma / D_t$ ²¹ to characterize the activity of ABPs and the area fraction $\phi = \pi \rho_0 \sigma^2 / 4$ to describe the density of ABPs with $\rho_0 = N / (L_x \times L_y)$ the averaged number density of the system. In simulations we set σ as the unit of length, $20k_B T$ as the unit of energy, and $\gamma \sigma^2 / (20k_B T)$ as unit of time. (See more details of the model in the Method section).

The phase diagram in the $\text{Pe} - \phi$ plane with interaction strength $\epsilon = 1$ is presented in Fig. 1a, wherein the color bar denotes the theoretical prediction of particle number fraction in dense phase $f_l = \frac{\rho_d \rho_0 - \rho_g}{\rho_0 \rho_d - \rho_g}$ (since the number density of dense phase ρ_d is not sensitive to the Péclet number and total density ρ_0 , we assume that ρ_d is constant and therefore, f_l only depends on ρ_g and ρ_0). It can be found that the simulated binodal (red dotted line) confirms with the phase boundary of the colored background predicted by our theoretical analysis. Likewise, theoretically predicted reentrance of MIPS can be observed as activity increases. For appropriate ϕ such as $\phi = 0.35$, the active system changes from a single phase to a coexisting phase and reenters to a single phase as Pe increases (typical snapshots can be found in Supplementary Fig. S1 in Supplementary Discussion I). Besides of the binodal, the spinodal (green dotted line) can also be obtained by simulations too. It can be found that both the binodal and spinodal curves shift to lower ϕ first, but reenter to higher ϕ again after an inflexion, forming a

brand new metastable state located in a much wider region at large Pe .

To investigate the nature of MIPS near the MIPS reentrance region, the growth process of the largest cluster (Fig. 1b) and a hysteresis loop (Fig. 1c) are focused. The inset of Fig. 1b plots time series of N_{max}/N with N_{max} the particle number of the largest cluster for ten independent simulations with $\phi = 0.35$ and $\text{Pe} = 900$ (time series for other parameters are shown in Supplementary Fig. S2 in Supplementary Discussion II). It can be observed that N_{max}/N increases from about 0 quickly after a waiting time t_w , indicating a first-order phase transition via nucleation²¹. Noticing that the waiting time can be a good parameter to measure the nucleation barrier, the obtained ensemble-averaged waiting time $\langle t_w \rangle$ as a function of Pe is then presented in Fig. 1b. As Pe increases across the upper spinodal, $\langle t_w \rangle$ increases exponentially, demonstrating that systems with larger Pe above the upper spinodal must go over a higher nucleation barrier to attain MIPS. Besides, a very large hysteresis loop with $\phi = 0.35$ can be found around the upper MIPS transition point as shown in Fig. 1c, demonstrating again the nucleation behavior of a discontinuous transition from a homogeneous initial state to MIPS²⁴. In short, the simulation results are consistent with our theoretical predictions, verifying that activity can bring unique phase behavior to the simplest ABP system.

Figure 2 a verifies the theoretical prediction about the effect of interaction strength ϵ on MIPS with fixed $\phi = 0.3$, where blue and red symbols indicate the single phase and the coexisting phase of MIPS, respectively. Phase boundaries between these two phases are the binodal (red lines), and the colored background is f_l obtained by our theoretical analysis. Clearly, the upper binodal increases remarkably as ϵ increases, while the lower binodal stays nearly unchanged. Such observation agrees with the theoretical prediction very well. To take a close look at the influence of ϵ , steady-state configurations of systems at $\text{Pe} = 2500$ and $\epsilon = 1.0, 1.5, 2.0$ and 4.0 are shown in Fig. 2b–e, respectively. As ϵ increases, the dense phase emerges with a relatively small cluster, and then grows to be a large cluster, indicating more and more pronounced MIPS. In other words, “harder” repulsive interactions between ABPs will lead to “weaker” reentrant MIPS while the “softer” ones will result in “stronger” reentrant MIPS, which further demonstrates the unique phase behavior induced by the nonequilibrium nature of activity.

Conclusion

In summary, reentrant MIPS induced solely by activity has been revealed. We showed both theoretically and numerically that such reentrant MIPS results from the competition between activity-induced effective attraction of ABPs preferring particle accumulation and activity-induced nonequilibrium vaporization hindering formation of large clusters. Our findings highlight the unique role played by the nonequilibrium nature of activity on phase behaviors of active systems, which may inspire deep insights into the essential difference between equilibrium and nonequilibrium systems.

Method

We consider a two-dimensional system with size $L_x \times L_y$ and periodic boundary conditions consisting of N spherical ABPs with diameter σ and friction coefficient γ . The motion of the i -th ABP located at \mathbf{r}_i obeys the following overdamped Langevin equations:

$$\dot{\mathbf{r}}_i = \nu_0 \mathbf{n}_i - \gamma^{-1} \sum_{j=1, j \neq i}^N \nabla_{\mathbf{r}_i} U(r_{ij}) + \xi_i, \quad (3)$$

$$\dot{\mathbf{n}}_i = \mathbf{n}_i \times \boldsymbol{\eta}_i. \quad (4)$$

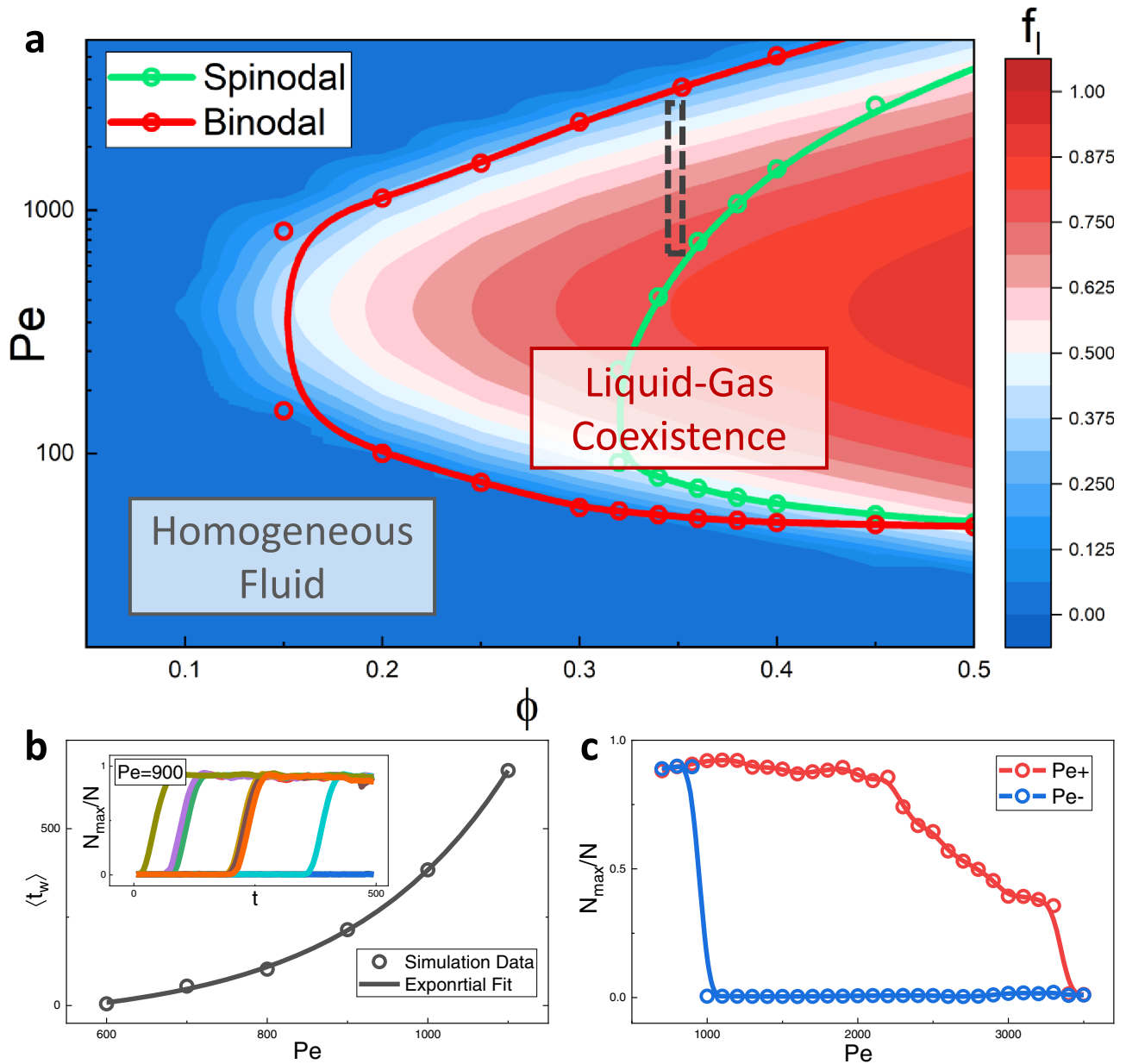


Fig. 1 The reentrant MIPS. **a** Phase diagram in the $Pe - \phi$ plane. The colored background is obtained by the kinetics model with $\lambda = 2.8 \times 10^{-4}$ and $\kappa = 0.9$. f_l is the fraction of dense phase. The red and green lines respectively represent the binodal and spinodal curves from simulations. **b** Dependence of the ensemble-averaged waiting time $\langle t_w \rangle$ for the nucleation on Pe for active systems at $\phi = 0.35$ inside the gray dashed box in **a**. Curves are the exponential fitting for the simulation data. The inset is the dependence of N_{max}/N with N_{max} the particle number of the largest cluster on t for ten independent ensembles at $\phi = 0.35$ and $Pe = 900$. **c** Hysteresis at $\phi = 0.35$ including the gray dashed box in **a**. Simulation data are reached from two initial conditions: the final configurations of systems at slightly smaller Pe (red line and symbols) and the ones at slightly larger Pe (blue line and symbols).

Herein, Eq. (3) represents the translational motion of the i -th ABP where v_0 and \mathbf{n}_i is respectively the amplitude and direction of active velocity. The interaction between a pair of ABPs is described by the purely repulsive Weeks–Chandler–Andersen (WCA) potential: $U(r_{ij}) = 4\epsilon[(\sigma/r_{ij})^{12} - (\sigma/r_{ij})^6 + 1/4]$ for $r_{ij} = |\mathbf{r}_i - \mathbf{r}_j| < 2^{1/6}\sigma$, and $U(r_{ij}) = 0$ otherwise, with ϵ the interaction strength. The last term ξ_i denotes the Gaussian white noise vector with time correlations $\langle \xi_i(t)\xi_j(t') \rangle = 2D_r \mathbf{I} \delta_{ij} \delta(t - t')$, where D_r is the translation diffusivity coefficient and \mathbf{I} is the unit matrix. We set $D_r = k_B T / \gamma$ so that the system satisfies the fluctuation-dissipation relation when propulsion forces are absent. Herein, k_B denotes the Boltzmann constant and T represents the temperature. Eq. (4) is the rotational equation of the i -th ABP. For a two-dimensional system, \mathbf{n}_i is confined into a two-dimensional space and only z -component (perpendicular to this plane) of the white noise η_i is concerned, which has time correlation $\langle \eta_i^z(t)\eta_j^z(t') \rangle = 2D_r \delta_{ij} \delta(t - t')$ where D_r is the rotational diffusivity coefficient which couples with the translational diffusivity $D_r = 3D_t/\sigma^2$.

In simulations, we use σ and $20k_B T$ respectively as basic units for length and energy, and set $\gamma = 1$ so that the basic unit for time is the $\gamma\sigma^2/(20k_B T)$. We fix $L_x = 800, L_y = 200, \epsilon = 1$, if not otherwise stated. In this work, we use two dimensionless parameters: the Péclet number $Pe = v_0\sigma/D_r$ to characterize the activity of ABPs and the area fraction $\phi = \pi\rho_0\sigma^2/4$ to describe the density of ABPs with $\rho_0 = N/(L_x \times L_y)$ the averaged number density of the system. For consistency, all of the following results are obtained from simulations of total time $t_{tot} = 500$ with the time step Δt changing from 10^{-5} to 10^{-6} for different activities. Notice that this volume fraction is only relevant on a parametric level, and does not correspond to the specific values of the hard sphere system. For active systems with Pe and ϕ located inside the spinodal curve, we ran simulations from random initial conditions. Whereas, for systems close to the binodal, as Pe increases(decreases), we used the final configurations of systems with slightly smaller(larger) Pe as the initial conditions for the ones with larger(smaller) Pe .^{21,24} In order to avoid finite-size effects especially at the large

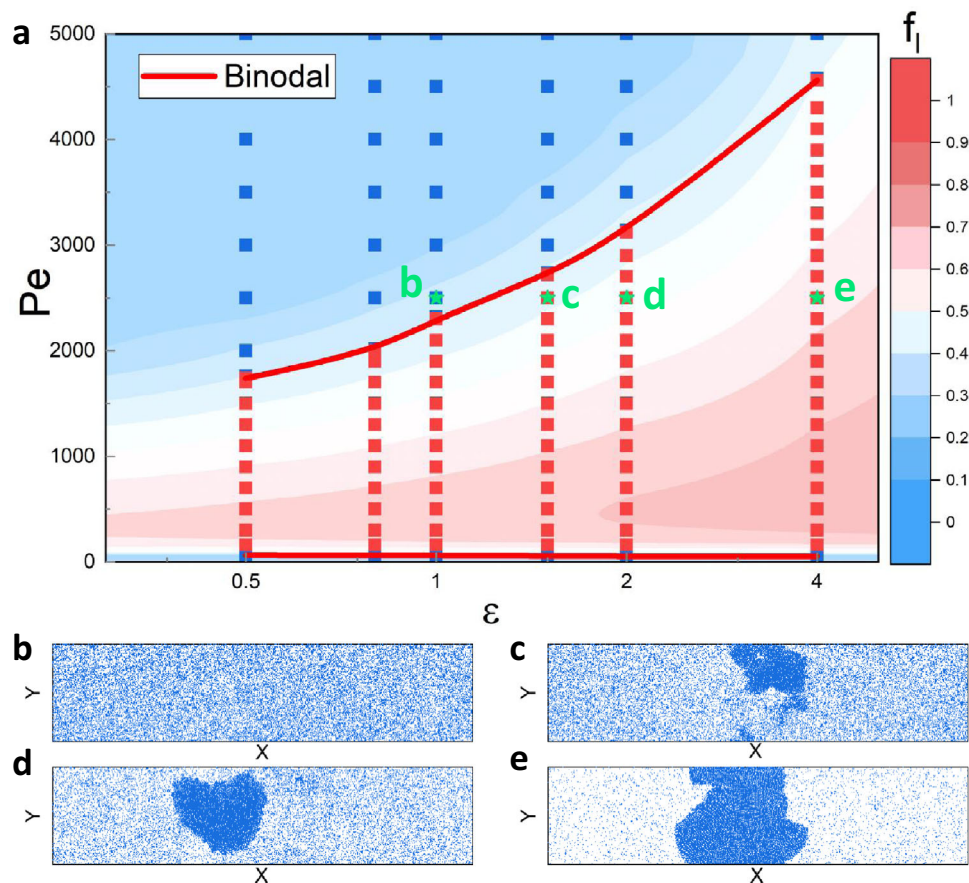


Fig. 2 Influence of the interaction strength. **a** Phase diagram in the $Pe - \epsilon$ plane at $\phi = 0.3$. The colored background is obtained by the kinetics model. The blue symbols represent the single phase, the red ones denote MIPS and the red-line boundaries is the binodal curves, which are all obtained by simulations. The steady-state configurations at $Pe = 2500$ and **b** $\epsilon = 1.0$, **c** 1.5 , **d** 2.0 and **e** 4.0 are respectively marked as green stars in **a**.

activity region, we have also made a number of simulations for larger systems, which are shown in Supplementary Discussion III.

Data availability

All data will be available from the authors upon request.

Code availability

The programming codes used for the numerical simulations will be available from the authors upon request.

Received: 4 May 2022; Accepted: 15 March 2023;

Published online: 31 March 2023

References

1. Bechinger, C. et al. Active particles in complex and crowded environments. *Rev. Mod. Phys.* **88**, 045,006 (2016).
2. Vicsek, T. & Zafeiris, A. Collective motion. *Phys. Rep.* **517**, 71–140 (2012).
3. Ramaswamy, S. The mechanics and statistics of active matter. *Annu. Rev. Condens. Matter Phys.* **1**, 323–345 (2010).
4. DiLuzio, W. R. et al. Escherichia coli swim on the right-hand side. *Nature* **435**, 1271 (2005).
5. Riedel, I. H., Kruse, K. & Howard, J. A self-organized vortex array of hydrodynamically entrained sperm cells. *Science* **309**, 300–303 (2005).
6. Kümmel, F. et al. Circular motion of asymmetric self-propelling particles. *Phys. Rev. Lett.* **110**, 198,302 (2013).
7. Gibbs, J., Kothari, S., Saintillan, D. & Zhao, Y. P. Geometrically designing the kinematic behavior of catalytic nanomotors. *Nano Lett.* **11**, 2543–2550 (2011).
8. Mallory, S. A. & Cacciuto, A. Activity-enhanced self-assembly of a colloidal Kagome lattice. *J. Am. Chem. Soc.* **141**, 2500–2507 (2019).
9. Gou, Y., Jiang, H. & Hou, Z. Assembled superlattice with dynamic chirality in a mixture of biased-active and passive particles. *Soft Matter* **15**, 9104–9110 (2019).
10. Du, Y., Jiang, H. & Hou, Z. Self-assembly of active core corona particles into highly ordered and self-healing structures. *J. Chem. Phys.* **151**, 154,904 (2019).
11. Yan, J. et al. Reconfiguring active particles by electrostatic imbalance. *Nat. Mater.* **15**, 1095 (2016).
12. Sumino, Y. et al. Large-scale vortex lattice emerging from collectively moving microtubules. *Nature* **483**, 448 (2012).
13. Jiang, H., Ding, H., Pu, M. & Hou, Z. Emergence of collective dynamical chirality for achiral active particles. *Soft Matter* **13**, 836–841 (2017).
14. Karani, H., Pradillo, G. E. & Vlahovska, P. M. Tuning the random walk of active colloids: from individual run-and-tumble to dynamic clustering. *Phys. Rev. Lett.* **123**, 208,002 (2019).
15. Gou, Y. L., Jiang, H. J. & Hou, Z. H. Emergent swarming states in active particles system with opposite anisotropic interactions. *Chin. J. Chem. Phys.* **33**, 717–726 (2020).
16. Jiang, H. & Hou, Z. Nonequilibrium dynamics of chemically active particles. *Chin. J. Chem.* **40**, 419–429 (2022).
17. Xu, R. K., Jiang, H. J. & Hou, Z. H. Simulation study of passive rod diffusion in active bath: nonmonotonic length dependence and abnormal translation-rotation coupling. *Chin. J. Chem. Phys.* **34**, 157–164 (2021).
18. Gou, Y. L., Jiang, H. J. & Hou, Z. H. Emergent swarming states in active particles system with opposite anisotropic interactions. *Chin. J. Chem. Phys.* **33**, 717 (2021).
19. Tailleur, J. & Cates, M. E. Statistical mechanics of interacting run-and-tumble bacteria. *Phys. Rev. Lett.* **100**, 218,103 (2008).
20. Cates, M. E. & Tailleur, J. Motility-induced phase separation. *Annu. Rev. Condens. Matter Phys.* **6**, 219–244 (2015).
21. Redner, G. S., Hagan, M. F. & Baskaran, A. Structure and dynamics of a phase-separating active colloidal fluid. *Phys. Rev. Lett.* **110**, 055,701 (2013).
22. Redner, G. S., Wagner, C. G., Baskaran, A. & Hagan, M. F. Classical nucleation theory description of active colloid assembly. *Phys. Rev. Lett.* **117**, 148,002 (2016).
23. Takatori, S. C. & Brady, J. F. Towards a thermodynamics of active matter. *Phys. Rev. E* **91**, 032,117 (2015).

24. Speck, T., Bialké, J., Menzel, A. M. & Löwen, H. Effective cahn-hilliard equation for the phase separation of active brownian particles. *Phys. Rev. Lett.* **112**, 218,304 (2014).
25. Speck, T., Menzel, A. M., Bialké, J. & Löwen, H. Dynamical mean-field theory and weakly non-linear analysis for the phase separation of active brownian particles. *J. Chem. Phys.* **142**, 224,109 (2015).
26. Tjhung, E., Nardini, C. & Cates, M. E. Cluster phases and bubbly phase separation in active fluids: Reversal of the ostwald process. *Phys. Rev. X* **8**, 031,080 (2018).
27. Takatori, S. C., Yan, W. & Brady, J. F. Swim pressure: stress generation in active matter. *Phys. Rev. Lett.* **113**, 028,103 (2014).
28. Zöttl, A. & Stark, H. Hydrodynamics determines collective motion and phase behavior of active colloids in quasi-two-dimensional confinement. *Phys. Rev. Lett.* **112**, 118,101 (2014).
29. Stenhammar, J., Wittkowski, R., Marenduzzo, D. & Cates, M. E. Activity-induced phase separation and self-assembly in mixtures of active and passive particles. *Phys. Rev. Lett.* **114**, 018,301 (2015).
30. Mandal, S., Liebchen, B. & Löwen, H. Motility-induced temperature difference in coexisting phases. *Phys. Rev. Lett.* **123**, 228,001 (2019).
31. Su, J., Jiang, H. & Hou, Z. Inertia-induced nucleation-like motility-induced phase separation. *N. J. Phys.* **23**, 013,005 (2021).
32. Du, Y., Jiang, H. & Hou, Z. Rod-assisted heterogeneous nucleation in active suspensions. *Soft Matter* **16**, 6434–6441 (2020).
33. Caprini, L., Bettolo Marconi, U. M. & Puglisi, A. Spontaneous velocity alignment in motility-induced phase separation. *Phys. Rev. Lett.* **124**, 078,001 (2020).
34. Caprini, L., Bettolo Marconi, U. M., Maggi, C., Paoluzzi, M. & Puglisi, A. Hidden velocity ordering in dense suspensions of self-propelled disks. *Phys. Rev. Res.* **2**, 023,321 (2020).
35. Onuki, A. *Phase transition dynamics* (Cambridge University Press, 2002)
36. Laughlin, D. E., Hono, K. *Physical metallurgy* (Newnes, 2014)
37. Vuijk, H. D., Brader, J. M. & Sharma, A. Effect of anisotropic diffusion on spinodal decomposition. *Soft Matter* **15**, 1319–1326 (2019).
38. Redner, G. S., Baskaran, A. & Hagan, M. F. Reentrant phase behavior in active colloids with attraction. *Phys. Rev. E* **88**, 012,305 (2013).
39. Takatori, S. C. & Brady, J. F. Swim stress, motion, and deformation of active matter: effect of an external field. *Soft Matter* **10**, 9433–9445 (2014).
40. Farage, T. F. F., Krinninger, P. & Brader, J. M. Effective interactions in active brownian suspensions. *Phys. Rev. E* **91**, 042,310 (2015).
41. Feng, M. & Hou, Z. Mode coupling theory for nonequilibrium glassy dynamics of thermal self-propelled particles. *Soft Matter* **13**, 4464–4481 (2017).

Acknowledgements

This work is supported by MOST(2018YFA0208702), NSFC (21973085, 21833007), Anhui Initiative in Quantum Information Technologies (AHY090200), and the Fundamental Research Funds for the Central Universities (WK2340000104).

Author contributions

Z.H. conceived the idea and designed the research. H.J. supervised the research. M.F. provided the theoretical model and analysis. J.S. performed the simulations and data analysis. Y.D. also performed the simulations. All authors discussed the results and co-wrote the manuscript.

Competing interests

The authors declare no competing interests.

Additional information

Supplementary information The online version contains supplementary material available at <https://doi.org/10.1038/s42005-023-01172-6>.

Correspondence and requests for materials should be addressed to Huijun Jiang or Zhonghuai Hou.

Peer review information *Communications Physics* thanks Ran Ni, Francisco Alarcon Oseguera and the other, anonymous, reviewer(s) for their contribution to the peer review of this work. Peer reviewer reports are available.

Reprints and permission information is available at <http://www.nature.com/reprints>

Publisher's note Springer Nature remains neutral with regard to jurisdictional claims in published maps and institutional affiliations.



Open Access This article is licensed under a Creative Commons Attribution 4.0 International License, which permits use, sharing, adaptation, distribution and reproduction in any medium or format, as long as you give appropriate credit to the original author(s) and the source, provide a link to the Creative Commons license, and indicate if changes were made. The images or other third party material in this article are included in the article's Creative Commons license, unless indicated otherwise in a credit line to the material. If material is not included in the article's Creative Commons license and your intended use is not permitted by statutory regulation or exceeds the permitted use, you will need to obtain permission directly from the copyright holder. To view a copy of this license, visit <http://creativecommons.org/licenses/by/4.0/>.

© The Author(s) 2023